1. Referee #2. The assumptions underlying h_{eq} and q do not satisfy current standards in the literature: h_eq is derived under the assumption of no motion, while the formulation of q excludes the region near the equator. The layer-thickness subcomponents associated with the rotational and divergent wind stress can be readily obtained by running the shallow-water model. The diagnostic expressions for the layer-thickness subcomponents should be discussed after their dynamical responses have been obtained from the shallow-water model.

The relative contributions of h_{eq} and q to the reconstructed Niño-3.4 variability are not quantified. In particular, since the manuscript attributes the long-term variability primarily to q, it would be useful to quantify and compare the low-frequency contributions from h_{eq} and q.

Authors.
We appreciate Referee #2's major comments, which we summarize as follows (see also point 14 of Referee #2): q-waves theory is derived under the geostrophic assumption, whereas h_{eq} is derived under the assumption of no motion. These assumptions may filter out high-frequency variability in both q and h_{eq}, thereby undermining the study's main hypothesis, according to which q-waves determine long-term SST variability, while equilibrium dynamics determine interannual variability.

To address these issues, let's start with h_{eq}. In responding to Referee #1 we defined "h_{eq} as the interface between the surface and bottom layer in equilibrium with the irrotational component of the DWS with the fluid at a hydrostatic or motionless state (u=0)" (see doi: https://doi.org/10.5194/egusphere-2026-2393-RC1). Here, we would like to address Referee #2 comment from a slightly, yet equivalent, perspective. Let's start by observing that the unconventional scaling of the wind stress used to introduce the DWS aims to obtain a scalar potential (and a streamline) with physical dimensions of LENGHT. So, we define

$$h_{eq} \equiv -\phi$$

(where the triple horizontal lines mean identical by definition). We will then look for solution *h* that fluctuate around h_{eq} by a quantity -q. From this definition, it follows that h_{eq} may be interpreted as "the interface between the surface and bottom layer in equilibrium with the irrotational component of the DWS with the fluid at an ideal hydrostatic or motionless state". This is because, by introducing the "hydrostatic velocity" **0**=(0,0) (see LeBlonde and Mysak, 1978, page 15, eq. 5.1), we have $\nabla h_{eq} + \nabla \Phi = \mathbf{0} = (\partial \mathbf{0}/\partial t + 2\boldsymbol{\Omega}\times\mathbf{0})/g'$.

So, to clarify the Reviewer's point, h_{eq} is chosen as a baseline reference state defined identically from the scalar potential Φ, rather than a simplified predictive state reached by dynamically averaging out fluid motion. By explicitly capturing the time-varying DWS scalar potential, it inherently retains all frequencies present in the irrotational wind field forcing.

However, to better clarify the role of h_{eq} in our analysis, we have also prepared for the benefit of the Referee one video ("Video1.avi"). This video can be downloaded from Google Drive at

Video1.avi:
https://drive.google.com/file/d/1rB6XZJ5D92hxWwCKJM7PWusN-kkkzxg1/view?usp=sharing

We used the Google Drive workspace because we are unsure whether the EGU Sphere workspace allows us to upload video files. We will try to upload them there, but, if necessary, the videos are available at the links above. The purpose of these videos, is to compare the structure and variability of the irrotational component of the DWS (i.e., $\Phi = -h_{eq}$) with the spatial structure and variability of the pycnocline depth computed, as discussed in Appendix B of the original manuscript, using IAP-CAS TS data. The Video shows the temporal variability of the two fields. Remarkably, Φ (right panel) captures the main features of the "real" pycnocline structure (left panel). However, before an El Niño event takes place, $h_{eq} = -\Phi$ does not capture, for instance, the two deeper lobes located off the equator in the western part of the basin. These regions are located approximately below the dipolar structure shown in Figure 4a of the original manuscript, west of 220°E. These structures are evidently associated with Sverdrup transport and thus cannot be resolved by h_{eq}.

As a consequence, we reassure Referee #2 that, by construction, h_{eq} contains all frequencies that characterize the DWS scalar potential, and this definition carries no risk of filtering out low-frequency variability.

The situation regarding q-waves is more complicated. Referee #2 is correct: q-waves are derived under the geostrophic assumption. This assumption is, of course, valid away from the equator, and thus it cannot capture the equatorward bending of wave rays associated with beta dispersion or account for the excitation of Rossby waves by equatorial and coastal Kelvin waves (see also point 13 of Referee #2). However, we wish to underline that this is an off-equatorial theory and that the processes mentioned by Referee #2 occur on timescales that are short compared with those considered in this study.

Meridional mass redistribution due to Sverdrup transport (i.e. $\beta V = [\mathrm{curl}(\boldsymbol{\tau})]_z/\rho$) depends on the density of the surface layer (ρ). Therefore, it is natural to investigate how slow changes in the density of the surface layer modulate the Sverdrup mass redistribution that slowly "recharges" the system.

The Sverdrup theory is a geostrophic theory and, over the past 30 years, it has provided an invaluable tool for understanding ENSO dynamics (e.g., Jin, 1997). The effectiveness of the geostrophic assumption in recharge–discharge theory has also been demonstrated by several observational studies, which show that El Niño preconditioning is characterized by off-equatorial heat accumulation (e.g., Ballester et al., 2016; Yang et al., 2025).

In this research, we are interested in evaluating how changes in stratification determine variability in Sverdrup transport over time scales longer than one year. Q-waves are a mechanism by which the ocean accommodates the thermocline under mass redistribution induced by Sverdrup transport. Here, we have excluded the equatorial region and chosen to restrict our attention to the area outside 2°S and 2°N. In general, the geostrophic approximation holds when the time scales involved (T) are such that

$$Ro = U/f \cdot L = 1/f \cdot T \ll 1$$

where Ro indicates the Rossby number, U is the characteristic horizontal velocity scale, L and T are the spatial and temporal scales of the phenomena under study, and f is the Coriolis parameter. In this research, we have chosen to restrict our attention to phenomena with characteristic time scales (T) longer than one year. At 2°S and 2°N, we have $f \approx \pm 5 \times 10^{-6}\ s^{-1}$. Taking T = 1 year = 365 × 24 × 3600 s, we have

$$Ro = U/f \cdot L = 1/f \cdot T \approx 0.0062$$

This demonstrates that, over time scales longer than one year, the geostrophic approximation holds and the geostrophic solution tends to represent the full shallow-water solution well.

For all these reasons, this research must be framed within classical ENSO theories and regarded as a natural complement to the recharge/discharge paradigm, with the aim of quantifying how changes in the stratification properties of the water column interact with the rotational component of the wind stress field to determine interannual-to-interdecadal variability in tropical Pacific SST.

As a further major point, Referee #2 suggests quantifying and comparing the low-frequency contributions to h of h_{eq} and q. We thank Reviewer #2 for this excellent suggestion, which we partially implemented in Figure 6 of the original manuscript. In that figure, the black dashed line represented N34 reconstructed by setting $h = heq - FL[q] = -\Phi - FL[q]$, where FL denotes a low-pass filter with a cutoff frequency of 1/10 $year^{-1}$. However, this observation only partially addresses Referee #2’s suggestion. In the new Figure 6 (see below), we added a dotted line, which represents the N34 obtained by setting $h = FL[heq] - FH[q] = -FL[\Phi] - FH[q]$, where FL denotes a low-pass filter with a cutoff frequency of 1/10 $year^{-1}$ and FH denotes a high-pass filter with the same cutoff frequency. To address Referee #2’s suggestion, the figure shown below will replace Figure 6 in the original manuscript. Comparing the green line in this figure with the black dotted line shows that heq determines N34 variability on time scales shorter than a decade, whereas q determines N34 variability on time scales longer than a decade.

To finally address Referee #2 criticism, we will perform the following changes:

1. To avoid confusion the title will be changed into

“Interannual-to-Interdecadal variability of the El Niño Southern Oscillation”

2. The discussion from L420 and L426 on h_{eq} will be changed. Of course, in the section between L258 and L264 of the paragraph entitled “Wind stress and Z_{15}: “quasi-balance” and residual mean dynamics” in which we define h_{eq}, will be rewritten in order to address Referee #1 and #2 concerns.

3. The discussion about the geostrophic assumption between L283 and L285 will be expanded accounting for the concepts quoted above.

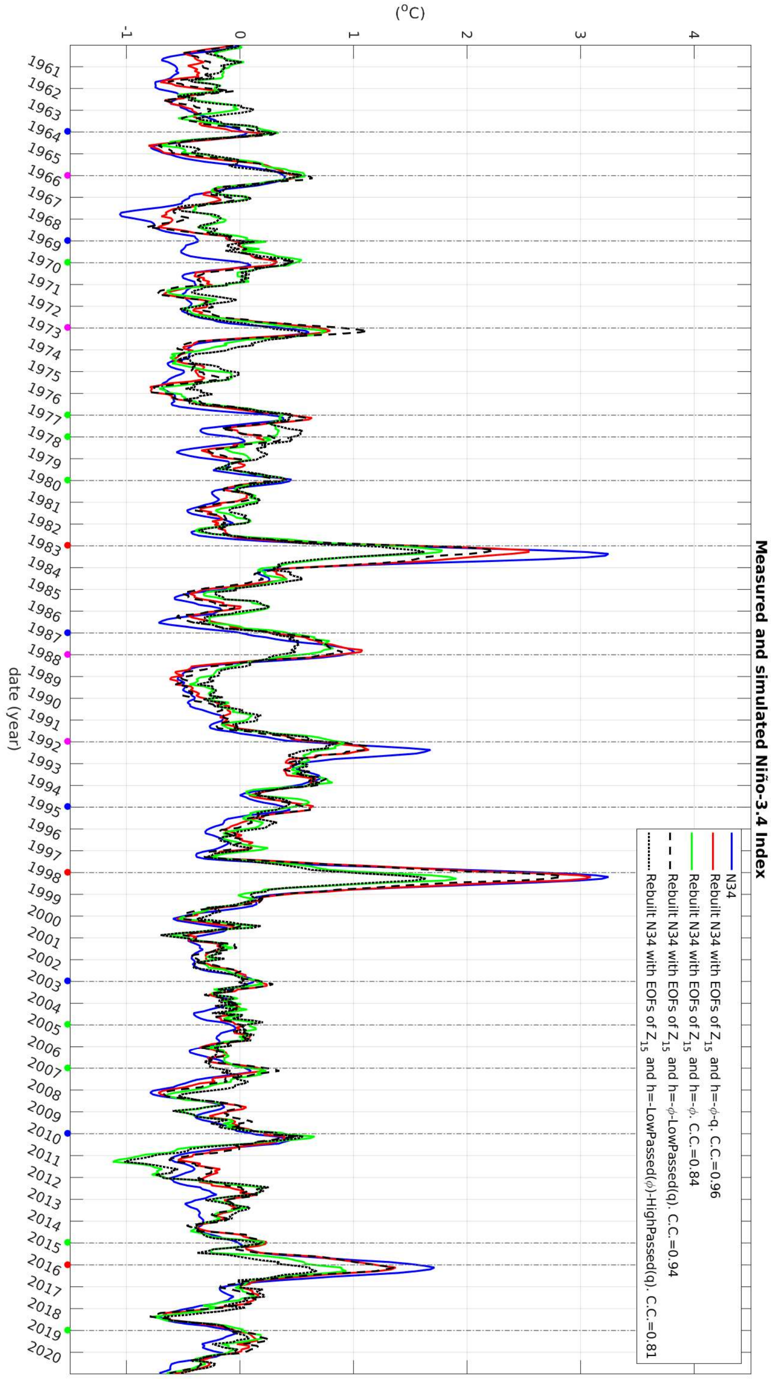

Figure 6: Measured (blue solid line) and simulated N_{34}. Red solid line: N_{34} simulated using the transfer function of Figure 1b and substituting, in place of the Z_{15} anomaly, the anomaly of the interface layer computed as $h = h_{eq} - q$. Green line: N_{34} simulated using the transfer function of Figure 1b and substituting, in place of the Z_{15} anomaly, the anomaly of the interface layer computed as $h = h_{eq}$ (same as green line of Figure 2). Black dashed line: N_{34} obtained from low passed q (frequency cut 1/10 years^{-1}). Black dotted line: N_{34} obtained from low passed heq and high passed q (frequency cut 1/10 years^{-1}). Colored dots on the horizontal bottom axis represent El Niño events classified as discussed in the legend of Figure 1a.

2. Referee #2. Figure 1a: Why does the Niño-3.4 index shown in Fig. 1a appear to have a substantial positive bias, with the La Niña events being systematically weaker? Compared with the Niño-3.4 index provided by the Copernicus Marine Service, the blue curve in Fig. 1a appears to be biased toward positive values. Please clarify the data source and processing used to obtain the Niño-3.4 index.

Authors.
Yes, indeed, Referee #2 is correct in raising a potential problem. However, we note that the problem is not with our data, except for the pre-satellite era, as we discussed in response to Point 1 of Referee #1 (https://doi.org/10.5194/egusphere-2026-2393-RC1), but with the fact that the data presented by Copernicus Marine Service (CMEMS; see https://data.marine.copernicus.eu/product/GLOBAL_OMI_CLIMVAR_enso_sst_area_averaged_anomalies/description) are the result of different processing and a different data source. Our N34 index is obtained from the ERA5 data set using a strict climatological prescription. Specifically, we downloaded ERA5 data from the Copernicus Climate Change Service (C3S; see L534–L535 of the original manuscript, not CMEMS). To compute the anomaly, we used the 30-year period from 1991 to 2020 as the climatological baseline (L175 of the original manuscript). The anomaly was then averaged over the Niño 3.4 region and filtered using a 5-month median filter. This is the standard procedure used in climate studies (see, for example, https://climatedataguide.ucar.edu/climate-data/nino-sst-indices-nino-12-3-34-4-oni-and-tni and Barnston et al., 1997). Note that the ERA5 SST data available from C3S are based on both satellite and in situ observations.

Conversely, the N34 index shown on the CMEMS website represents the SST anomaly relative to a climatological baseline computed over a 22-year period (i.e., 1993–2014). CMEMS then averages this anomaly over the Niño 3.4 region and removes the temporal mean without applying any data filtering. Furthermore, and more importantly, to compute N34, CMEMS uses the GLOBAL_MULTIYEAR_PHY_ENS_001_031 data set (see https://data.marine.copernicus.eu/product/GLOBAL_MULTIYEAR_PHY_ENS_001_031/description). This data set is the result of modeling exercises, and it has recently been observed that operational climate models often significantly overestimate the strength and likelihood of La Niña (Tan et al., 2025; Shen et al., 2026).

Therefore, it is not surprising that the N34 presented on the CMEMS website overestimates La Niña conditions and provides slightly different information from our N34 index. However, for the reasons cited above, the N34 index shown on the CMEMS website should be interpreted with caution and cannot be considered a “reference truth” for ERA5 data.

3. Referee #2. Figure 1a, 2b and 3: The ticks on the horizontal axis are difficult to read.

Authors.
Yes, we apologize for this. Referee #1 also made a similar comment. At the time of the original submission, we thought it was possible to submit full-resolution figures directly, rather than only figures inserted into the main text. We apologize for this misunderstanding. However, also in response to Referee #1’s request, all ticks, labels, and legends have been enlarged in all figures. We hope this will produce satisfactory graphical results.

4. Referee #2. Figure 2b: The ticks on the vertical axis are difficult to read.

Authors.
Please see authors comment to point 3 of Referee #2.

5. Referee #2. Line 192: It is unclear whether Z represents the interannual variability after removing the monthly climatology, or the raw (unprocessed) Z field.

Authors.
Sorry, we are afraid we do not understand. In the original manuscript we read in L192: "...In this equation $Z(x_m,t)$ represents the Z_{15} anomaly at point x_i on date *t*,…". So, Z represents the interannual variability after removing the monthly climatology.

6. Referee #2. Line 201: Please clarify whether the climatological and interannual components are treated together or separately in the analysis.

Authors.
As observed in addressing Point 5 of Referee #2, Z represents the Z_{15} anomaly.

7. Referee #2. Line 202, 388: A conventional alternative would be to perform an EOF analysis of the Z15 field (or SSH, SST) and examine the correlations between Niño-3.4 and the leading PCs (PC1, PC2, etc.). What are the advantages of the method adopted in this study compared with this conventional approach?

Authors.
Referee #2 is correct in raising this point. Typically, if one is interested in statistically analyzing how individual modes—each of which explains a fraction of the variance in a given field (say, X)—influence the variability of another field (say, Y), one performs an EOF analysis and compares the PCs of the two fields using statistical tools such as correlation analysis, Granger causality, and/or convergent cross-mapping. So, Referee #2 is correct: this is the standard approach for testing correlation and causality. However, in this case, we are not interested in testing correlation or causality between the Z_{15} anomaly and N34. Such a test would be quite naive, as it is well known that changes in thermocline depth in the tropical Pacific are closely related to changes in SST. Our objective, instead, is to define a transfer function that maps the Z_{15} anomaly to N34. To address this issue, we use, as noted by Referee #1, a fairly standard approach, namely least-squares fitting. As shown in Appendix A of the original manuscript, the coefficients, $w(x_i)$, that minimize the RMS error between N34 and its representation in terms of $Z(x_i,t)$ (Equations (1)–(3) of the original manuscript) are expressed in terms of the EOFs of the Z_{15} anomaly field, but this is simply the result of the least-square minimization procedure.

8. Referee #2. Line 255: Defining h_{eq} by considering a stationary state may be useful as a second choice. This assumption effectively excludes the dynamical contribution of propagating waves, such as equatorial Kelvin waves. The manuscript initially appears to examine the dynamics of Z_{15}, but the subsequent analysis bypasses the mathematical symmetry of rotational and divergent contributions. The authors should clarify this point and its physical implications.

Authors.
We believe we have already addressed this issue extensively in our response to Referee #2's main concerns. Therefore, to address this point, we refer to the first part of our response to Point 1 from Referee #2.

9. Referee #2. Line 265: The terminology used in the main text, the figure title, and the figure caption is inconsistent, which is confusing for the reader. In addition, the potential anomaly and h_{eq} should have opposite signs according to the definition given in the manuscript. Please make the terminology and sign convention consistent throughout the text and figures.

Authors.
Yes, indeed, we apologize for this. There was confusion in the original manuscript; see also, for instance, the new Figure 6 that we have added to this letter. We noticed inconsistencies in the legend

and corrected them. Thank you for making this point. In the revised manuscript, legends, titles, and captions will be corrected where necessary.

10. Referee #2. Eqs. (5) and (6): The notation c_n and c_m can easily be confused with c_1 in Eq. (7). Please use distinct notation to avoid this ambiguity.

Authors.
Yes, thank you for pointing this out: we did not notice that we used the same notation to represent the velocity of the first internal mode, c_1, in equation (7) and the coefficients in equations (5) and (6), which describe the transfer function, c_m. Sorry about that. In the new version of the manuscript, the coefficients in equations (5) and (6) will be referred to as a_m.

11. Referee #2. Eq. (7): It is unclear whether $\boldsymbol{\tau}$ represents the interannual variability after removing the monthly climatology, or the raw (unprocessed) $\boldsymbol{\tau}$ field.

Authors.
Sorry, but we are afraid we do not understand this point. In L243 of the original manuscript, right below eq. (7), we read: "...In equation (7), $\boldsymbol{\tau}$ represents the wind stress, *g'* the reduced gravity…" so it is the raw $\boldsymbol{\tau}$ field.

12. Referee #2. Line 244: It would be useful to mention here that previous studies have suggested that the second baroclinic mode is more closely associated with Niño-3 variability.

Authors.
This is indeed another excellent point raised by Referee #2 and it highlights a weakness of this study, namely the double-layer approximation. In general, although the ocean has effectively infinite vertical degrees of freedom, global current-meter observations and altimetric analyses confirm that kinetic energy and sea-surface-height variations across most of the world ocean are dominated by the barotropic and first baroclinic modes (Stammer, 1997; Wunsch, 1997; de La Lama et al., 2016; LaCasce, 2017). These results indicate that, in general, the dynamics of the world ocean can be described reasonably well in terms of an equivalent two-layer ocean system. However, Referee #2 is correct: although canonical ENSO theories adopt a two-layer description of the tropical Pacific vertical structure, it has been shown that in the eastern part of the basin the second baroclinic mode intensifies and is important for ENSO description (Dewitte et al., 1999; Dewitte et al., 2002; Cravatte et al., 2003; Dewitte and Moon, 2004). Although we focus on the N34 region, this is a limitation of our study in the eastern part of the basin and will be discussed before introducing the shallow-water, two-layer model (equation 8, before L249 of the original manuscript).

13. Referee #2. Eq. (10): Its present form permits Rossby waves to propagate only westward and cannot capture the equatorward bending of wave rays associated with beta dispersion. A further concern is that Eq. (10) cannot account for the excitation of Rossby waves by equatorial and coastal Kelvin waves that propagate around the eastern boundary of the Pacific. Thus, the present formulation does not capture all wind-driven themocline variations associated with the rotational or divergent components of the wind stress.

Authors.
This point has been addressed in responding to Point 1 from Referee #2. Please refer to Authors comment in that point.

14. Referee #2. Line 325: The quantity q will be obtained by time-integrating Eq. (8) with ϕ=0.

Authors.
Thanks for the very appropriate suggestion: extending q-wave theory to include high-frequency variability in wind-stress curl. However, given the time scales involved in this research, which are interannual to interdecadal, solving the full shallow-water equations would add substantial technical complexity without providing significant additional insight. As we noted in our response to Point 1 from Referee #2, the Rossby number over these time scales is approximately Ro ≈ 0.006, indicating that the geostrophic approximation is very appropriate for describing the relationship between the depth of the main thermocline and SST variability in the central Pacific over the time-scales involved in this research.

That said, the formulation proposed by Referee #2 forms the basis of a compelling, separate project. We are eager to explore this extension following the publication of this manuscript and warmly invite the reviewer, if so wished, to connect with us to collaborate on this future work. Specifically, in off-tropical regions, internal Rossby waves are derived from quasi-geostrophic potential vorticity conservation. Rossby waves arise from meridional variations in the Coriolis parameter (the β-effect). However, in the derivation of Rossby waves, the density field is assumed to be uniform and time independent. Horizontal gradients and temporal variability in surface density produce spatial gradients and temporal variability in the reduced-gravity field (see Figure 3 of the original manuscript). This variability acts as a separate source of vorticity that, together with wind-stress curl, forces pseudo-Rossby internal waves whose propagation properties vary spatially and under climate change. To investigate this, we are using the reduced-gravity dataset employed in this study, which was obtained as described in Appendix B, as well as data provided by IAP-CAS (see L176–L181 of the original manuscript).

References

Ballester, J., S. Bordoni, D. Petrova, and X. Rodó (2016). Heat advection processes leading to El Niño events as depicted by an ensemble of ocean assimilation products, J. Geophys. Res. Oceans, 121, 3710–3729, doi:10.1002/2016JC011718.

Barnston, A. G., Chelliah, M., & Goldenberg, S. B. (1997). Documentation of a highly ENSO-related SST region in the equatorial Pacific: Research note. Atmosphere-ocean, 35(3), 367-383.

Cravatte, S., Picaut, J., & Eldin, G. (2003). Second and first baroclinic Kelvin modes in the equatorial Pacific at intraseasonal timescales. Journal of Geophysical Research: Oceans, 108(C8), 3266.

de La Lama, M. S., LaCasce, J. H. & Fu, L.-L. (2016). The vertical structure of ocean eddies. Journal of Climate System 1, dzw001.

Dewitte, B., Reverdin, G., & Maes, C. (1999). Vertical structure of an OGCM simulation of the equatorial Pacific Ocean in 1985–1994. Journal of Physical Oceanography, 29(7), 1542-1570.

Dewitte, B., Schneider, N., Perigaud, C., Chang, P., & Thual, O. (2002). On the importance of subsurface variability for ENSO simulation and prediction. Geophysical Research Letters, 29(14), 1666

Dewitte, B., & Moon, B. K. (2004). Vertical structure variability in the equatorial Pacific before and after the late 1970s climate shift. Geophysical Research Letters, 31(3).

LaCasce, J. H. (2017). The prevalence of oceanic surface modes. Geophysical Research Letters 44, 10-537.

LeBlond P.H. and L.A. Misak (1978). Waves in the Ocean. Elseevier Oceanography Series.

Shen, J.-Y, Fei Zheng, F., Chao-Fan Li, C.-F. (2026). Key physical processes of the 2024 La Niña suppression from the perspective of air–sea antagonism, Atmospheric and Oceanic Science Letters, https://doi.org/10.1016/j.aosl.2026.100885.

Stammer, D. (1997). Global characteristics of ocean variability estimated from regional TOPEX/POSEIDON altimeter measurements. J. Phys. Oceanogr. 27, 1743-1769.

Tan, W., Hu, Z. Z., Liu, Y., & McPhaden, M. J. (2025). Evolution and prediction of the La Niña conditions in 2024/25. Environmental Research Communications, 7(12), 125031.

Yang, G., Jin, Y., Zhao, Y., Di Lorenzo, E., McPhaden, M. J., & Lin, X. (2025). Improving ENSO prediction at longer lead times: Role of off-equatorial South Pacific heat content. Geophysical Research Letters, 52, e2024GL114540. https://doi.org/10.1029/2024GL114540

Wunsch, C. (1997). The vertical partition of oceanic horizontal kinetic energy. Journal of Physical Oceanography 27, 362 1770–1794.